Optics Communications 448 (2019) 10–14

Contents lists available at ScienceDirect

Optics Communications

journal homepage: www.elsevier.com/locate/optcom

Intrinsically or extrinsically reconfigurable chirality in plasmonic chiral metasurfaces

Shengtao Yin [a,b], Wei Ji [a,*], Dong Xiao [b], Yu Li [a], Ke Li [b], Zhen Yin [b], Shouzhen Jiang [c], Liyang Shao [b], Dan Luo [b], Yan Jun Liu [b,*]

[a] School of Information Science and Engineering, Shandong University, Qingdao 266237, China
[b] Department of Electrical and Electronic Engineering, Southern University of Science and Technology, Shenzhen 518055, China
[c] School of Physics and Electronics, Shandong Normal University, Jinan 250014, China

ARTICLE INFO

Keywords:
Chirality
Metasurface
Plasmonics
Liquid crystals
Reconfigurability

ABSTRACT

In this work, we theoretically present a reconfigurable plasmonic chiral metasurface based on a sandwiched metal–insulator–metal structure, which can strongly, spin-selectively absorb circularly polarized light. Through finite-difference time-domain simulation, the absorption of left- or right-handed circularly polarized light can reach nearly 100% at the resonant position, and the magnitude of the circular dichroism can be 80%, which is larger than most of the previously reported value. This strong chiroptical effect originates from plasmonic resonances induced by the incident circularly polarized light. Furthermore, the proposed plasmonic chiral metasurface is able to be reconfigurable by either changing its intrinsic or extrinsic chirality, which can be numerically confirmed by the change of the sign and magnitude of the CD. Such a reconfigurable plasmonic chiral metasurface could find many potential applications in chirality detection/sensing, polarimetric imaging, spin–orbit communications, etc.

1. Introduction

An object with chirality refers to the fact that its geometry cannot be overlapped by its mirror images. In nature, chirality is ubiquitous and widely exists in different forms ranging from quartz crystals, proteins, acids to galaxies. One fascinating property of chiral media is that they show different response to circularly polarized light (CPL) with different spin states. Such phenomena typically term chiroptical effects including optical activity and circular dichroism (CD). However, chirality in natural chiral media are usually weak so that it cannot provide an efficient way to manipulate the spin state of the light. In recent years, thanks to the advance of nanofabrication, this dilemma could be solved by plasmonic metamaterials. By artificially designing chiral building blocks, plasmonic metamaterials can exhibit greatly enhanced chirality that is not available in natural chiral materials [1–3]. Chiral plasmonic metamaterials have already demonstrated several intriguing properties such as giant optical activity and CD [4–9], chirality-induced negative refraction [10,11], and asymmetric transmission [12,13]. They have also found important applications including chirality detection, polarimetric imaging, spin–orbit communications, and so on [14–17]. One distinctive property of chiral plasmonic metamaterials is the pronounced CD [18–21], which is several orders of magnitude larger than that of natural chiral media. CD is defined as the difference in absorption between left and right circularly polarized (LCP and RCP) light, which has vital applications in various disciplines. For example, CD spectroscopy serves as a powerful technique in biomedicine, chemistry and pharmacy. It can analyze structural, conformational, and thermodynamic properties of chiral molecules. Metasurfaces are two-dimensional counterparts of metamaterials. Recently, chiral metasurfaces become more attractive due to their ultrathin feature yet excellent control on the phase and the CPL polarization state at deep subwavelength scale [22,23]. Chiral metasurface can support strong CPL-matter interaction and lead to the maximum CD (One spin state of CPL is totally absorbed while the other one is totally reflected/transmitted) [24–26].

However, most of the reported chiral metasurfaces are unreconfigurable. The functionality is fixed once the structures are designed and fabricated, which greatly limits their applications. One of the most important yet challenging requirements for real applications is to make the chiral metasurfaces active. To this end, intensive effort has been made to realize the reconfigurability or tunability [27–31]. In principle, the active control can be achieved by changing the intrinsic or extrinsic chirality [32–35]. For example, Giessen group demonstrated a reconfigurable plasmonic chiral metamaterial based on the phase change material GST-326 [36]. By controlling the temperature, GST-326 could change its phase from amorphous phase to crystalline phase and the corresponding refractive index is changed. As a result, the

* Corresponding authors.
E-mail addresses: jiwww@sdu.edu.cn (W. Ji), yjliu@sustech.edu.cn (Y.J. Liu).

https://doi.org/10.1016/j.optcom.2019.05.006
Received 21 January 2019; Received in revised form 30 April 2019; Accepted 6 May 2019
Available online 10 May 2019

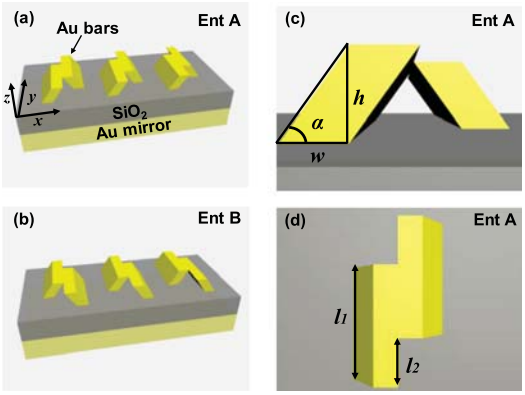

Fig. 1. Schematic illustration of the plasmonic chiral metasurface with its unit cell consisting of two slanted gold bars at the top layer and a gold mirror placed at the bottom of a SiO_2 layer. (a, b) The pair enantiomers of the plasmonic chiral metasurface that are labeled as Ent A and Ent B, respectively. (c, d) The side and top views of Ent A show the important structural parameters.

large tunable range of the CD response is achieved in mid-infrared regime by changing the intrinsic chirality. Zheludev group designed an array of non-chiral metal split rings to generate the strong CD effect in GHz regime, which is coined as extrinsic chirality [37]. They measured losses and phase retardation for CPL transmitted by the metamaterial at different incident angles from −30° to +30° achieved by tilting the structure around its symmetry axis, which have confirmed reconfigurable resonant extrinsic chiral optical effect in a non-chiral planar metamaterial.

In this work, we theoretically propose a reconfigurable plasmonic chiral metasurface that is based on a sandwiched metal–insulator–metal *(MIM)* structure. The proposed chiral metasurface has highly spin-selective absorption, resulting a strong CD. The sign and magnitude of the CD can be dynamically reconfigured via changing either the intrinsic or extrinsic chirality. The proposed reconfigurable plasmonic chiral metasurface provides an efficient approach to manipulate the CPL state and could find many potential applications in chirality detection/sensing, polarimetric imaging, spin–orbit communications, etc.

2. Design and theoretical analysis

The chiroptical effects originate from the cross coupling between magnetic and electric fields for both natural and artificial media. As illustrated in Fig. 1, to achieve large chirality, we propose a chiral metasurface with its unit cell consisting of two slanted gold bars. A gold mirror placed beneath the gold bars separated by a dielectric (SiO_2) layer. The top Au structure layer is surrounded by air. Figs. 1(a) and 1(b) shows the pair of enantiomers that are labeled as Ent A and Ent B, respectively. Figs. 1(c) and 1(d) shows the detailed structural parameters of a unit cell with the periods of $p_x = 300$ nm and $p_y = 400$ nm. The two gold bars have the same thickness of $h = 100$ nm, width of $w = 50$ nm, and length of $l_1 = 200$ nm, respectively. The slanted angle of each gold bar is $\alpha = 16°$ and the staggered distance between the two gold bars is $l_2 = 100$ nm. The thickness of SiO_2 dielectric layer is 500 nm. The thickness of the gold mirror was set to be 100 nm, which is much larger than its skin depth so as to ensure that there is no transmission. All the proposed structural dimensions are the optimized parameters by considering the practicability of the experimental realization.

To investigate the physical mechanism and chiroptical response of the metasurface, we utilized the finite-difference time-domain (FDTD) method to calculate the reflection spectra as well as the electromagnetic field distribution [38]. The single unit of the nanostructure was simulated with Bloch boundary conditions along x- and y-directions and perfectly matched layer (PML) along z-direction. The mesh size in the simulation was set to be 5 nm in all directions. The dispersion property of gold is taken from Johnson and Christy model [39].

The refractive index of the SiO_2 dielectric layer is set as 1.45. The incident CPL can be considered as the superposition of two orthogonal linearly polarized light that oscillates with 90° phase shift, and hence can be written as [40]:

$$E_{RCP} = (E_x, E_y)^T = (\frac{\sqrt{2}}{2}, \frac{\sqrt{2}}{2} e^{\frac{\pi}{2} i})^T \tag{1}$$

$$E_{LCP} = (E_x, E_y)^T = (\frac{\sqrt{2}}{2}, \frac{\sqrt{2}}{2} e^{-\frac{\pi}{2} i})^T \tag{2}$$

E_x and E_y are the linearly polarized electric fields along x- and y-directions, respectively. Via the superposition of reflected linearly polarized light, we can obtain the reflection complex coefficients of the incident CPL. Their relationship can be well described by the advanced Jones matrix [41,42]. The reflection matrix for a circular polarization state can be written as:

$$\begin{aligned} R &= \begin{bmatrix} \beta_{LR} & \beta_{LL} \\ \beta_{RR} & \beta_{RL} \end{bmatrix} = \frac{1}{2} \begin{bmatrix} 1 & 1 \\ i & -i \end{bmatrix} \begin{bmatrix} \beta_{xx} & \beta_{xy} \\ \beta_{yx} & \beta_{yy} \end{bmatrix} \begin{bmatrix} 1 & 1 \\ i & -i \end{bmatrix} \\ &= \frac{1}{2} \begin{bmatrix} \beta_{xx} + \beta_{yy} + i(\beta_{xy} - \beta_{yx}) & \beta_{xx} - \beta_{yy} - i(\beta_{xy} + \beta_{yx}) \\ \beta_{xx} - \beta_{yy} + i(\beta_{xy} + \beta_{yx}) & \beta_{xx} + \beta_{yy} - i(\beta_{xy} - \beta_{yx}) \end{bmatrix} \end{aligned} \tag{3}$$

In above equations, β denotes the reflection coefficients, the first and second subscripts of β refer to the reflected and incident waves and L/R refer to LCP/RCP as viewed along the z-direction. In this way, we can analyze all the components of the reflected RCP and LCP light: $R_R = |\beta_{RR} + \beta_{RL}|$, $R_L = |\beta_{LR} + \beta_{LL}|$. Note that x and y refer to the orthogonal linearly polarized light with the polarization along x- and y-directions, respectively.

3. Results and discussion

The CD can be calculated as $CD = |A_{RCP} - A_{LCP}|$. Due to the energy conservation law, $A = 1 - T - R$. Since the gold mirror is thick enough, the transmission is totally blocked. Therefore, CD can be also simplified as $CD = |R_{RCP} - R_{LCP}|$. Figs. 2(a) and 2(b) depicts the reflection and CD spectra for LCP and RCP light within the wavelength range from 600 to 900 nm for both Ent A and B. We can see a giant difference in reflection between LCP and RCP at ~650 nm, indicating strong chirality. The chiral metasurface structures Ent A and B have nearly unit absorption for the incident LCP and RCP, respectively. The simulated CD is more than 70%. To understand the underlying mechanism of the chiroptical response, the detailed four components of the β matrix are further calculated. Due to the $C2$ symmetry of the chiral nanostructure, R matrix in the circular representation can be given as [40]:

$$R = \begin{bmatrix} \beta_{LR} & \beta_{LL} \\ \beta_{RR} & \beta_{RL} \end{bmatrix} = \frac{1}{2} \begin{bmatrix} \beta_{xx} + \beta_{yy} & \beta_{xx} - \beta_{yy} - i(\beta_{xy} + \beta_{yx}) \\ \beta_{xx} - \beta_{yy} + i(\beta_{xy} + \beta_{yx}) & \beta_{xx} + \beta_{yy} \end{bmatrix} \tag{4}$$

Fig. 2(c) and 2(d) exhibits the calculated results of simulation. Since we have $R_{RL} = R_{LR}$, the corresponding curves are completely overlapped. The strong CD effect is mainly attributed to the components, R_{RR} and R_{LL}. That is to say, the reflected or absorbed CPL is caused by the same state of the incident CPL, which is quite different from the regular mirror. In comparison with the MIM structure, we also carried out the simulation for the top Au structure alone and the achieved results are shown in Fig. 2(e). We can see that the Au structure itself only demonstrates a weak chiroptic effect. The CD value is ~20%, which is far less than that of the MIM structure (nearly 80%). Obviously, the MIM structure forms a resonant cavity that amplifies the plasmonic resonance and further enhance the chiral effect significantly.

The spin-selective absorption arises from the excitation of plasmonic resonance modes in the chiral metasurface, which is induced by charge oscillation and accumulation on the metal–insulator interface. In order to further understand the physical mechanism, we calculate the induced

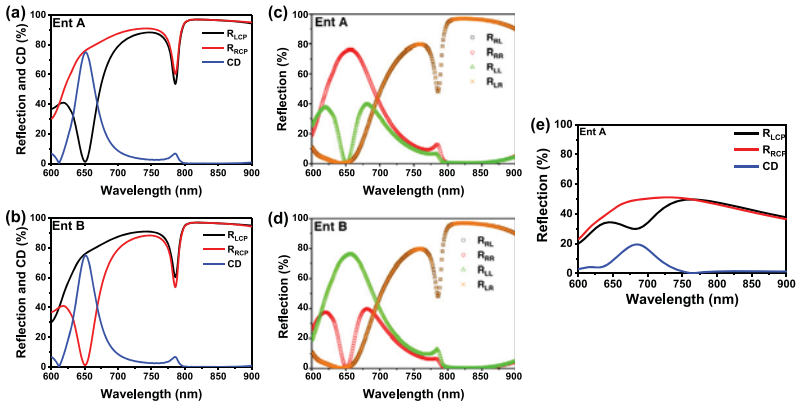

Fig. 2. Simulated reflection and CD spectra of the plasmonic chiral metasurface for Ent A (a) and B (b). The reflection spectra of the LCP and RCP components for Ent A (c) and B (d). *The reflection spectra of the LCP and RCP components for Ent A (e) with the slanted gold-bar structure alone.*.

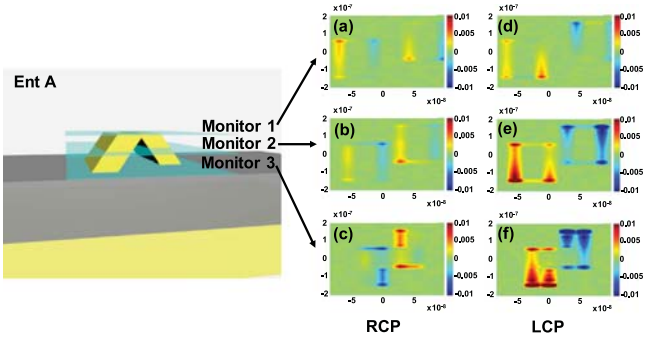

Fig. 3. The induced charge distributions of Ent A at three different monitoring positions with the left and right panels for the incident RCP and LCP light, respectively. The corresponding resonant wavelength is 650 nm.

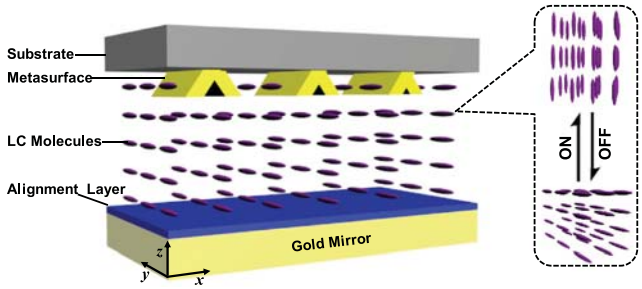

Fig. 4. Schematic of the chiral metasurface (Ent A) integrated with LCs. The right part shows the respective alignment of LC molecules at "OFF" and "ON" states driven by an applied voltage. Incident light propagates through the metasurface and LC layer along $-z$-direction.

charge distribution at the resonant wavelength of 650 nm. Fig. 3 depicts the corresponding charge distributions of Ent A at three different planes of $h_1 = 100$ nm (Fig. 3(a) and 3(d)), $h_2 = 50$ nm (Fig. 3(b) and 3(e)) and $h_3 = 0$ nm (Fig. 3(c) and 3(f)) from the top surface of SiO_2 dielectric layer. For better comparison, the color scale bars are set to be same for all mappings. We can then see obvious differences of the charge distributions under the LCP and RCP light illumination. The charge accumulation mainly occurs at the nanostructure's edges and corners, confirming that the observed optical response results mainly from the plasmonic resonances. For structure Ent A, it is obvious that the LCP-induced charge distributions in the right panel is much stronger than the RCP-induced ones in the left panel, resulting in a strong chiroptical effect, which is in good agreement with the results in Fig. 2(a). The different resonant position manifests that the resonant modes are highly dependent on the CPL spin state, while the charge distribution of the other areas can be neglectable. The CPL absorption is principally attributed to the ohmic dissipation of the induced current, which leads to the drastically different absorption, reflection and large CD.

3.1. Intrinsic chirality-induced reconfigurability

Up to now, most of reported chiral metasurfaces cannot be reconfigurable (i.e., only passive) without changing the physical dimensions of nanostructures, which is disadvantageous for many applications. To overcome this issue, one feasible method is to integrate active materials with the passive chiral metasurfaces. In this regard, liquid crystals (LCs) could be an ideal candidate for designing reconfigurable chiral metasurfaces due to their large birefringence, versatile driving methods and wide working frequency window [43–46].

For convenient integration of the chiral metasurface with LCs, we replace the SiO_2 dielectric layer with a LC layer in the previous design. The resulted design is schematically shown in Fig. 4. With this design, the gold bar nanostructures can be fabricated on a separate conductive substrate. A thin polyvinyl alcohol (PVA) layer can be spin-coated on the gold mirror for LC alignment. A nematic LC, E7 [47,48], was used with its ordinary and extraordinary refractive indices being well described by the extended Cauchy model [49]. *In our numerical simulation, we use an anisotropic medium model to simulate the LC. The wavelength-dependent dispersion of the LC E7 was calculated using the extended Cauchy model and then used for FDTD simulations in our proposed LC-based chiral metasurface.* The LC E7 has a large birefringence with its ordinary refractive index of $n_o = 1.5211$ and extraordinary refractive index of $n_e = 1.7464$ at 20 °C.

As known, the plasmonic resonance is highly sensitive to the surrounding dielectric medium [50–52]. In our design, the LC molecules can be reoriented by an externally applied voltage, hence resulting in the change of the effective refractive index of the LC layer and making the plasmonic chiral metasurface reconfigurable. In addition, since the orientation of the LC molecules is not perpendicular to the x-y plane, the refractive indices experienced by the x- and y-polarized light are different, which will further cause the x- and y-polarized light to propagate at different velocities through the LCs layer. The induced phase retardation can be given as [53]:

$$\Delta\varphi = \frac{2\pi h \left| n_e - n_o \right|}{\lambda} \tag{5}$$

The phase retardation $\Delta\varphi$ is proportional to the thickness of the LC layer h. When $\Delta\varphi = \pi$, the spin state of the incident CPL could be then completely changed to the other opposite state by designing the proper thickness of the LC layer, leading to the sign change of CD and the spin

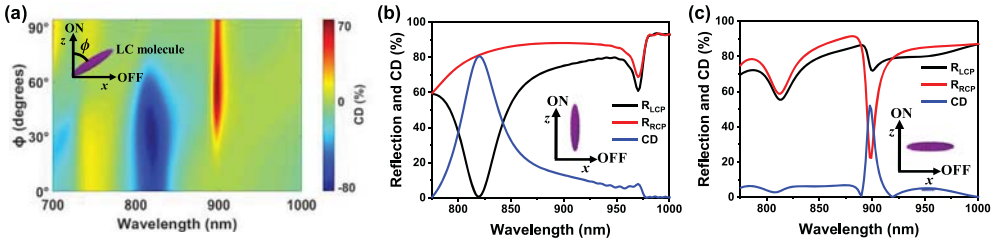

Fig. 5. (a) The CD mapping with the tilting angle of the LC molecules under the CPL illumination. Simulated reflection and CD spectra of the LC-integrated plasmonic chiral metasurface at "ON" (b) and "OFF" (c) conditions.

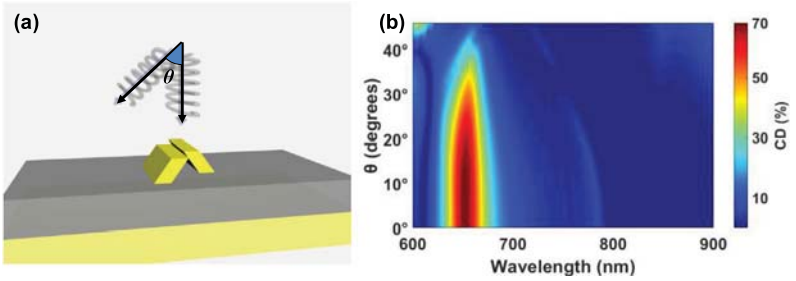

Fig. 6. (a) Schematic of the incident CPL on the plasmonic chiral metasurface. The incident angle of CPL varies from 0 to 45°. (b) The calculated CD mapping as a function of incident angle.

change of the CPL absorption. These characteristics make the integrated chiral metasurface reconfigurable by changing its intrinsic chirality.

Fig. 5(a) shows the calculated magnitude and sign of the CD as a function of the tilting angle of the LC molecules. Note that in Fig. 5(a), we followed the convention to define the CD as $CD = A_{RCP} - A_{LCP} = R_{LCP} - R_{RCP}$, indicating that the sign of the CD can vary from positive to negative, and vice versa. For the sake of comparison, we used the absolute value of the CD elsewhere in this work without further mentioning. The tilting angle ϕ of the LC molecules can be changed from 0° ("ON" condition) to 90° ("OFF" condition) by an externally applied voltage, as shown in the inset of Fig. 5(a). We can see that due to the realignment-induced the change of the effective index of the LCs, the LC-integrated plasmonic chiral metasurface shows different CD responses. According to Eq. (5), if we chose the resonant wavelength of $\lambda \approx 900$ nm, and set $\Delta\varphi$ and $|n_e - n_o|$ as π and 0.2, respectively, the required thickness of the LC layer can be then estimated to be ~2200 nm. Due to the fact that the incident CPL is reflected back to the LC layer upon the gold mirror, the actual LC layer will be only half of the estimated thickness, i.e., ~1100 nm. Figs. 5(b) and 5(c) exhibits the reflection and CD spectra for LCP and RCP light. At "ON" condition, the calculated CD is more than 80% and the absorption is nearly 100% for the incident LCP light. At "OFF" condition, due to the inhomogeneous refractive index, although the result is not as good as the "ON" condition, the achieved CD is still larger than 50%. With the decreased ϕ from 90° to 0° (i.e., from "OFF" condition to "ON" condition), the magnitude of CD response varies accordingly and the sign of CD is also flipped. Due to the change of the LCs' effective refractive index, the resonant wavelength also shifts. Hence, the LC-integrated plasmonic chiral metasurface is reconfigurable via changing its intrinsic chirality by externally applying a voltage.

3.2. Extrinsic chirality-induced reconfigurability

Due to the oblique CPL incidence, the time of the light propagating through different areas of the chiral metasurface structure is unequal. For some specially designed metasurface structures, the difference of the asymmetric absorption between the incident RCP and LCP light can produce significant CD. The phase difference of the resonant modes stimulated by the two CPL spin states results in strong interferences of the modes. It leads to different absorption between the LCP and RCP incidence to achieve the extrinsic chirality. With the above optimized design, we further check the dependence of CD on the incident angle θ, as shown in Fig. 6. From Fig. 6(b), we can see clearly that with the increase of the incident angle, the CD gradually decreases. At the incident angle of 45°, the CD effect nearly disappears. As a result, we could then make the plasmonic chiral metasurface reconfigurable by changing its extrinsic chirality via varying the incident CPL angle.

4. Conclusion

In summary, we have numerically demonstrated a reconfigurable chiral metasurface based on a sandwiched MIM structure. The FDTD simulation results showed that one spin state of specific CPL can be completely absorbed by the metasurface, and the magnitude of the CD can be more than 80%. In addition, by either changing the CPL incident angle or integrating the metasurface with nematic LCs, the sign and magnitude of the CD can be dynamically reconfigured. Such a reconfigurable plasmonic chiral metasurface could find many potential applications in chirality detection/sensing, polarimetric imaging, spin–orbit communications, etc.

Acknowledgments

This work was financially supported by National Natural Science Foundation of China (Grant Nos. 61571273, 61771292, 61805113), National Key Research and Development Program of China (Grant No. 2017YFC0803403), Natural Science Foundation of Shandong Province of China (Grant No. ZR2016FM29), Natural Science Foundation of Guangdong Province, China (Grant No. 2017A030313034 and 2018A030310224), Shenzhen Science and Technology Innovation Commission, China (Grant No. JCYJ20170817111349280) and the Program for Guangdong Introducing Innovative and Enterpreneurial Teams, China (Grant No. 2017ZT07C071).

References

[1] J.J. Cheng, E.H. Hill, Y.B. Zheng, T.C. He, Y.J. Liu, Optically active plasmonic resonance in self-assembled nanostructures, Mater. Chem. Front. 2 (2018) 662–678.

[2] E.S.P. Leong, J. Deng, E.H. Khoo, S.J. Wu, W.K. Phua, Y.J. Liu, Fabrication of free-standing three-dimensional chiral plasmonic nanostructures with single-step electron-beam lithography, RSC Adv. 5 (2015) 96366–96371.
[3] J.K. Gansel, M. Wegener, S. Burger, S. Linden, Gold helix photonic metamaterials: a numerical parameter study, Opt. Express 18 (2010) 1059–1069.
[4] M. Kuwata-Gonokami, N. Saito, Y. Ino, M. Kauranen, K. Jefimovs, T. Vallius, J. Turunen, Y. Svirko, Giant optical activity in quasi-two-dimensional planar nanostructures, Phys. Rev. Lett. 95 (2005) 227401.
[5] A.B. Khanikaev, N. Arju, Z. Fan, D. Purtseladze, F. Lu, J. Lee, P. Sarriugarte, M. Schnell, R. Hillenbrand, M.A. Belkin, G. Shvets, Experimental demonstration of the microscopic origin of circular dichroism in twodimensional metamaterials, Nature Commun. 7 (2016) 12045.
[6] S.P. Rodrigues, S. Lan, L. Kang, Y. Cui, P.W. Panuski, S. Wang, A.M. Urbas, W. Cai, Intensitydependent modulation of optically active signals in a chiral metamaterial, Nature Commun. 8 (2017) 14602.
[7] M. Saba, M. Thiel, M.D. Turner, S.T. Hyde, M. Gu, K. Grosse-Brauckmann, D.N. Neshev, K. Mecke, G.E. Schröder-Turk, Circular dichroism in biological photonic crystals and cubic chiral nets, Phys. Rev. Lett. 106 (2011) 103902.
[8] E.H. Khoo, E.S.P. Leong, S.J. Wu, W.K. Phua, Y.L. Hor, Y.J. Liu, Effects of asymmetric nanostructures on the extinction difference properties of actin biomolecules and filaments, Sci. Rep. 6 (2016) 19658.
[9] W.K. Phua, Y.L. Hor, E.S.P. Leong, Y.J. Liu, E.H. Khoo, Study of circular dichroism modes through decomposition of planar nanostructures, Plasmonics 11 (2016) 449–457.
[10] J.B. Pendry, A chiral route to negative refraction, Science 306 (2004) 1353–1355.
[11] S. Zhang, Y.S. Park, J. Li, X. Lu, W. Zhang, X. Zhang, Negative refractive index in chiral metamaterials, Phys. Rev. Lett. 102 (2009) 023901.
[12] C. Menzel, C. Helgert, C. Rockstuhl, E.B. Kley, A. Tünnermann, T. Pertsch, F. Lederer, Asymmetric transmission of linearly polarized light at optical metamaterials, Phys. Rev. Lett. 104 (2010) 253902.
[13] A.S. Schwanecke, V.A. Fedotov, V.V. Khardikov, S.L. Prosvirnin, Y. Chen, N.I. Zheludev, Nanostructured metal film with asymmetric optical transmission, Nano Lett. 8 (2008) 2940–2943.
[14] E. Hendry, T. Carpy, J. Johnston, M. Popland, R.V. Mikhaylovskiy, A.J. Lapthorn, S.M. Kelly, L.D. Barron, N. Gadegaard, M. Kadodwala, Ultrasensitive detection and characterization of biomolecules using superchiral fields, Nat. Nanotechnol. 5 (2010) 783–787.
[15] R. Farshchi, M. Ramsteiner, J. Herfort, A. Tahraoui, H.T. Grahn, Optical communication of spin information between light emitting diodes, Appl. Phys. Lett. 98 (2011) 162508.
[16] G.A. Hembury, V.V. Borovkov, Y. Inoue, Chirality-sensing supramolecular systems, Chem. Rev. 108 (2008) 1–73.
[17] G. Bautista, M. Decker, M. Wegener, M. Kauranen, M.J. Huttunen, S. Linden, Nonlinear chiral imaging of subwavelength-sized twisted-cross gold nanodimers, Opt. Mater. Express 1 (2011) 46–56.
[18] Z. Fan, H. Zhang, A. Govorov, Plasmonic circular dichroism of chiral nanoparticle assemblies, Nano Lett. 10 (2010) 2580–2587.
[19] T. Cao, C. Wei, L. Mao, Y. Li, Extrinsic 2d chirality: giant circular conversion dichroism from a metal–dielectric-metal square array, Sci. Rep-UK 4 (2014) 7442.
[20] T. Cao, C. Wei, L. Zhang, Modeling of multi-band circular dichroism using metal/dielectric/metal achiral metamaterials, Opt. Mater. Express 4 (2014) 1526–1534.
[21] T. Cao, M.J. Cryan, Enhancement of circular dichroism by a planar non-chiral magnetic metamaterial, J. Opt. 14 (2012) 085101.
[22] V.K. Valev, J.J. Baumberg, B. De Clercq, N. Braz, X. Zheng, E.J. Osley, S. Vandendriessche, M. Hojeij, C. Blejean, J. Mertens, C.G. Biris, V. Volskiy, M. Ameloot, Y. Ekinci, G.A.E. Vandenbosch, P.A. Warburton, V.V. Moshchalkov, N.C. Panoiu, T. Verbiest, Nonlinear superchiral meta-surfaces: Tuning chirality and disentangling non-reciprocity at the nanoscale, Adv. Mater. 26 (2014) 4074–4081.
[23] G.X. Li, S. Zhang, T. Zentgraf, Nonlinear photonic metasurfaces, Nat. Rev. Mater. 2 (2017) 17010.
[24] T. Cao, L. Zhang, R.E. Simpson, C. Wei, M.J. Cryan, Strongly tunable circular dichroism in gammadion chiral phase-change metamaterials, Opt. Express 21 (2013) 27841–27851.
[25] B. Tang, Z. Li, E. Palacios, Z. Liu, S. Butun, K. Aydin, Chiral-selective plasmonic metasurface absorbers operating at visible frequencies, IEEE Photon. Technol. Lett. 29 (2017) 295–298.
[26] Y. Qu, L. Huang, L. Wang, Z. Zhang, Giant circular dichroism induced by tunable resonance in twisted Z-shaped nanostructure, Opt. Express 25 (2017) 5480–5487.
[27] T. Cao, Y. Li, X. Zhang, Y. Zou, Theoretical study of tunable chirality from graphene integrated achiral metasurfaces, Photonics Res. 5 (2017) 441–449.
[28] T. Cao, C. Wei, L. Mao, S. Wang, Tuning of giant 2d-chiroptical response using achiral metasurface integrated with graphene, Opt. Express 23 (2015) 18620–18629.
[29] T. Cao, Y. Li, L. Tian, H. Liang, K. Qin, Fast switching on/off chiral surface plasmon polaritons in graphene-coated Ge2Sb2Te5 nanowire, ACS Appl. Nano Mater. 1 (2018) 759–767.
[30] S.T. Yin, D. Xiao, J.X. Liu, K. Li, H.L. He, S.Z. Jiang, D. Luo, X.W. Sun, W. Ji, Y.J. Liu, Reconfigurable chiral metasurface absorbers based on liquid crystals, IEEE Photon. J. 10 (2018) 4600909.
[31] D. Xiao, Y.J. Liu, S.T. Yin, J.X. Liu, W. Ji, B. Wang, D. Luo, G.X. Li, X.W. Sun, Liquid-crystal-loaded chiral metasurfaces for reconfigurable multiband spin-selective light absorption, Opt. Express 26 (2018) 25305–25314.
[32] A. Yokoyama, M. Yoshida, A. Ishii, Y.K. Kato, Giant circular dichroism in individual carbon nanotubes induced by extrinsic chirality, Phys. Rev. X 4 (2014) 331–344.
[33] X. Lu, J. Wu, Q. Zhu, J. Zhao, Q. Wang, L. Zhan, W. Ni, Circular dichroism from single plasmonic nanostructures with extrinsic chirality, Nanoscale 6 (2014) 14244–141253.
[34] M.V. Mukhina, V.G. Maslov, A.V. Baranov, A.V. Fedorov, A. Orlova, F. Purcellmilton, J. Govan, Y.K. Gun'ko, Intrinsic chirality of CdSe/ZnS quantum dots and quantum rods, Nano Lett. 15 (2015) 2844–2851.
[35] X.J. Liu, I.P. Hamilton, A series of intrinsically chiral gold nanocage structures, Nanoscale 9 (2017) 10321–10326.
[36] X. Yin, M. Schäferling, A.K.U. Michel, A. Tittl, M. Wuttig, T. Taubner, H. Giessen, Active chiral plasmonics, Nano Lett. 15 (2015) 4255–4260.
[37] E. Plum, V.A. Fedotov, N.I. Zheludev, Optical activity in extrinsically chiral metamaterial, Appl. Phys. Lett. 93 (2008) 191911.
[38] D.M. Sullivan, Electromagnetic Simulation Using the FDTD Method, IEEE Press, 2013.
[39] P.B. Johnson, R.W. Christy, Optical constants of the noble metals, Phys. Rev. B 6 (1972) 4370–4379.
[40] A.K. Jin, Research Topics in Electromagnetic Wave Theory, Wiley, 1981.
[41] C. Menzel, C. Rockstuhl, F. Lederer, An advanced jones calculus for the classification of periodic metamaterials, Phys. Rev. A 82 (2010) 3464–3467.
[42] Z. Wang, H. Jia, K. Yao, W. Cai, H. Chen, Y. Liu, Circular dichroism metamirrors with near-perfect extinction, ACS Photon. 3 (2016) 2096–2101.
[43] S. Yin, Y.J. Liu, D. Xiao, H. He, D. Luo, S.Z. Jiang, H.T. Dai, W. Ji, X. Sun, Liquid-crystal-based tunable plasmonic waveguide filters, J. Phys. D: Appl. Phys. 51 (2018) 235101.
[44] Y.J. Liu, G.Y. Si, E.S.P. Leong, N. Xiang, A.J. Danner, J.H. Teng, Light-driven plasmonic color filters by overlaying photoresponsive liquid crystals on gold annular aperture arrays, Adv. Mater. 24 (2012) 131–135.
[45] Y.J. Liu, Q.Z. Hao, J.S.T. Smalley, J. Liou, I.C. Khoo, T.J. Huang, A frequency-addressed plasmonic switch based on dual-frequency liquid crystals, Appl. Phys. Lett. 97 (2010) 091101.
[46] G.Y. Si, Y.H. Zhao, E.S.P. Leong, Y.J. Liu, Liquid-crystal-enabled active plasmonics: A review, Materials 7 (2014) 1296–1317.
[47] J. Li, S.T. Wu, S. Brugioni, R. Meucci, S. Faetti, Infrared refractive indices of liquid crystals, J. Appl. Phys. 97 (2005) 073501.
[48] M. Ma, S.G. Li, X.L. Jing, H.L. Chen, Refractive indices of liquid crystal e7 depending on temperature and wavelengths, Opt. Eng. 56 (2017) 117109.
[49] J. Li, S.T. Wu, Extended Cauchy equations for the refractive indices of liquid crystals, J. Appl. Phys. 95 (2004) 896–901.
[50] E.S.P. Leong, Y.J. Liu, J. Deng, Y.T. Fong, N. Zhang, S.J. Wu, J.H. Teng, Fluid-enabled significant enhancement and active tuning of magnetic resonances in free-standing plasmonic metamaterials, Nanoscale 6 (2014) 11106–11111.
[51] M.S. Wang, C.L. Zhao, X.Y. Miao, Y.H. Zhao, J. Rufo, Y.J. Liu, T.J. Huang, Y.B. Zheng, Plasmofluidics: Merging light and fluids at the micro-/nano-scale, Small 11 (2015) 4423–4444.
[52] K. Chen, E.S.P. Leong, M. Rukavina, T. Nagao, Y.J. Liu, Y.B. Zheng, Active molecular plasmonics: Tuning surface plasmon resonances by exploiting molecular dimensions, Nanophotonics 4 (2015) 186–197.
[53] E. Hecht, Optics, Addison Wesley Longman Inc, 2001.